

Global Minimum For A variant Mumford-Shah Model with Application to medical image Segmentation

Da Chen*, Mingqiang Yang[†], Laurent D. Cohen*

*CEREMADE UMR CNRS 7534, Universite Paris Dauphine, France

Email: {chenda, cohen}@ceremade.dauphine.fr

[†]school of Information Science and Engineering, Shandong University, China

Email: yangmq@sdu.edu.cn

Abstract

Traditional level set-based active contour models/snakes are widely applied to medical image segmentation. The main problems faced by those traditional models are that they cannot find the global minimum of the energy functionals and hardly handle the intensity inhomogeneities which often occur in medical images. In order to overcome the drawbacks mentioned above, we make use of a global minimization framework and the dual formulation of the total variation (TV) norm to solve a global variant Mumford-Shah energy with bias field estimator. Furthermore, we utilize a new method to compute the bias field estimator by the Gaussian kernel function, which can ensure the bias field estimator to keep smooth in the whole image domain. Finally, through the dual projection method of the weighted TV-norm, we can find the global minimum of the variant Mumford-Shah energy with bias field estimator rather than the local one. Experimental results demonstrate that our method can obtain the desire results both in synthetic and medical images.

Keywords

Medical Image Segmentation; Tubular Structure Segmentation; Active Contour Model; Global Minimum; Dual Formulation;

I. INTRODUCTION

Medical image segmentation forms the critical basis of various diseases diagnoses and treatment. Unfortunately, it still faces many difficulties for traditional edge detection methods in automatically segmenting the medical images like vascular images because of the presence of intensity inhomogeneities and the effect of noise. Actually, intensity inhomogeneities often arise from technical limitations or artifacts introduced by the objects, which can be solved by more sophisticated models. Recently, variational methods, especially for active contour models (ACM) have been widely applied to the medical images with the presence of intensity inhomogeneities and complex background [?], [?].

The classical parametric ACMs [?], [?], [?] consisting of minimizing an energy functional to drive contours toward the boundaries of objects can obtain closed curves as segmentation results. However, those parametric models are dependent of the curve's parameterization and cannot automatically handle topological changes. Geometric ACMs [?], [?] based on the level set method [?] were proposed to overcome the drawbacks of the parametric ACMs, and utilize only geometric measures for curves evolution toward the boundaries. Both parametric and geometric edge-based ACMs using the image gradients as the objects boundaries are roust to intensity inhomogeneities.

Work on region-based active contour models are inspired by the Mumford-Shah model [?] which is a very important problem in terms of image segmentation. However, it is difficult to find numerical approximations and implementations. T. Chan et al. proposed a piecewise constant Mumford-Shah model called C-V model which used a constant to approximate each image component [?]. With the application of variational level set method [?], the C-V method is easy to apply to homogeneous image segmentation. L. vese et al. [?] and Andy Tsai et al. [?] use the curve evolution technique to solve the piecewise smooth Mumford-Shah problem [?]. Li. et al. [?] proposed to use local binary fitting (LBF) to replace the fitting constants of the C-V model. Brox et al. [?] and Lanktona et al. [?] proposed a local region-based ACMs combined with Gaussian kernel function to reduce the computational time of the piecewise smooth model [?], [?], which often fall into a local minimum. Li. et al. [?] proposed a local cluster (LC) method with bias field estimator to solve the initialization sensitivity problem of the local region model. Jung et al. [?], [?] proposed a nonlocal active contour model utilizing Euclidean and Wasserstein distances between pairs of patches within each region to construct the energy.

The main drawback of the level set-based ACMs is that they can only find the local (non-global) minimum which often leads to false results. To deal with this problem, L. Cohen et.al proposed a minimal paths approach [?] to find the global minimum of the snake energy among all paths between two points provided by users. The model is formulated as minimizing the integral of a feature potential P among all curves that join the two user supplied points. However, it is difficult for the global minimal path method to find a closed curve as segmentation result. F. Benmansour et al. [?] proposed a method by automatically introducing new end points which are called keypoints. Those keypoints can be initially reduced to only one starting point. The main issue of this method is that it is difficult to give a relevant stopping criterion to decide when to stop the iterations.

T. Chan et al. [?] proposed a new variational framework to find the global minimum of the C-V model [?]. In this framework, the level set formulation is replaced by a new convex set so that global minimum can be achieved because of the convexity of the energy functional. Bresson et al. [?] unified the piecewise constant model and piecewise smooth model into the variational framework of [?] to carry out the global minimum of the corresponding active contour energy and solve the problem of the active curve propagation through a fast dual projection method [?]. Other interesting active contour methods have been presented in [?], [?], [?], [?], [?], [?], [?].

In this paper, we propose a variant Mumford-Shah model with bias field estimator for medical image segmentation, where the global minimum can be found by the method presented in [?]. In our method, the bias field estimator of the images can be calculated by Gaussian kernel functional. Due to the effect of the bias field estimator and the new variational framework proposed by T. Chan [?], the proposed method can handle the intensity inhomogeneities and find the global minimum of the variant Mumford-Shah model. Experimental results comparing with the level set method (presented in section IV) demonstrate that our method outperforms the widely used method, like [?], [?], [?].

The paper is organized as follows: In section II, we will introduce the original Mumford-Shah model [?] serving as preliminary model to our approach and its reduced piecewise constant case, i.e., the C-V model. Section III will present the proposed formulation including the Gaussian kernel-based bias field computing method as well as the global minimum for the proposed model. Section IV will explain the experimental results both in synthetic and medical images. Section V will give the conclusion.

II. RELATED WORKS

The important segmentation problem formulated by Mumford and Shah [?] can be defined as follows: Given an observed image $I : \Omega \rightarrow R$ (Ω is an open subset in R^2), the Mumford-Shah model is to find all the connected components Ω_i of Ω and boundaries $\partial\Omega_i, i = 1, 2, 3 \dots N$. Such that, a piecewise smooth approximation u is found by minimizing the following energy functional, where u varies smoothly within each Ω_i .

$$E^{MS}(u, C) = \int_{\Omega} (I - u)^2 dx + \mu \int_{\Omega \setminus C} |\nabla u|^2 dx + \nu |C| \quad (1)$$

where μ, ν are positive weighting constants and $|C|$ denotes the length of curve C . Minimizing term $\int_{\Omega \setminus C} |\nabla u|^2 dx$ and $|C|$ is to ensure u and curve C to keep smooth, respectively. In (??), the approximation u can be smooth only inside each region component Ω_i . Existence and regularity of minimizers of (??) can be achieved theoretically [?]. L.vese et al. [?] and Tsai et al. [?] solved the minimization problem of (??) by the variational level set method [?] and curve evolution technique, making the piecewise smooth Mumford-Shah model be widely applied to image segmentation.

T. Chan et al. [?] introduced the C-V model which is considered as an efficient numerical implementation scheme for the Mumford-Shah functional by assuming that $\mu \rightarrow \infty$, i.e., the piecewise smooth approximation u can be restricted to a piecewise constant. The C-V model is a reduced case of Mumford-Shah functional:

$$E^{CV} = \mu \left(\int_{\Omega_1} (I - c_1)^2 dx + \int_{\Omega_2} (I - c_2)^2 dx \right) + \nu |C| \quad (2)$$

where μ and ν are positive parameters. Ω_1 and Ω_2 are the image regions outside and inside the curve(s) C , respectively. The Constants c_1 and c_2 are the region fitting data, which can be computed by

$$c_1 = \frac{\int_{\Omega_1} I(x) dx}{\int_{\Omega_1} dx}, \quad c_2 = \frac{\int_{\Omega_2} I(x) dx}{\int_{\Omega_2} dx} \quad (3)$$

The C-V functional (??) will achieve its minimum if c_1 and c_2 formulated in (??) can approximate the image outside and inside the curves C well, i.e.,

$$\int_{\Omega_1} (I - c_1)^2 dx \approx \int_{\Omega_2} (I - c_2)^2 dx \approx 0 \quad (4)$$

The C-V formulation can be easily solved by taking the Euler-Lagrange equations as well as the variational level set framework [?]. However, one main problem is that the C-V model cannot handle the intensity inhomogeneities as it assumes that the images can be divided into piecewise constant region components.

III. GLOBAL MINIMUM FOR VARIANT MUMFORD-SHAH MODEL WITH BIAS FIELD

A. Image Model

As mentioned above, intensity inhomogeneity often occurs in medical images due to the technical limitations or artifacts introduced by the objects. In this paper, our method is mainly based on the following image model:

$$I(x) = B(x)T + n, \quad x \in \Omega_i, \quad i = 1, 2 \dots N. \quad (5)$$

where n is additive noise and N is the total number of region components Ω_i (for two-phase segmentation, $N = 2$). This image model is formulated for images based on that an observed image I can be represented as a product of the true image data T and a bias field estimator B varying slowly. A guided filtering introduced in [?] is also based on the guidance image T and makes use of a locally affine version of true image T . In this paper, the true image data T can be formulated as [?]:

$$T = \sum_i c_i \chi_i, \quad i = 1, 2 \dots N \quad (6)$$

where c_i is a constant and χ_i is the the characteristic function of components Ω_i . Based on the image model (??), our aim is to find the bias field estimator B and the true image T . In the following section, we present a method to compute the bias field estimator B by a Gaussian kernel function which can keep B varying slowly in the whole image domain Ω .

B. Variant Mumford and Shah mode with bias field estimator

Let $I : \Omega \rightarrow R$ be the image to be segmented and χ_i be the characteristic function of region components $\Omega_i, i = 1, 2$, where $\chi_2 = 1 - \chi_1$. Replacing the piecewise smooth approximation u by (??), we can obtain the following formulation [?], [?]:

$$u(x) = \sum_i B(x)c_i\chi_i, \quad x \in \Omega_i, \quad i = 1, 2 \quad (7)$$

Based on the formulation of the Mumford and Shah model in (??) and image model in (??), the variant Mumford and Shah mode with bias field estimator can be formulated as follows:

$$\begin{aligned} E^{vms} = & \lambda(\int_{\Omega_1}(I(x) - Bc_1)^2 dx + \int_{\Omega_2}(I(x) - Bc_2)^2 dx) \\ & + \mu \int_{\Omega} |\nabla B|^2 dx + \nu |C| \end{aligned} \quad (8)$$

where λ, μ and ν are weighting parameters. The third term $\mu \int_{\Omega} |\nabla B|^2 dx$ is to ensure the bias field estimator to keep smooth in Ω and the last term $\nu |C|$ is the curve length which is used to keep the active curve(s) C smooth. Combined with the characteristic functions χ_1 and χ_2 , the energy shown in (??) can be rewritten as follows:

$$\begin{aligned} E^{vms}(c_1, c_2, B) = & \lambda \int_{\Omega} ((I - Bc_1)^2 \chi_1 + (I - Bc_2)^2 \chi_2) dx \\ & + \mu \int_{\Omega} |\nabla B|^2 dx + \nu |C| \end{aligned} \quad (9)$$

Minimization of energy (??) can be solved by alternate minimization, for example the iterative process method [?]. For each iteration, energy (??) can be minimized by three steps:

- a) For fixed characteristic function χ_1, χ_2 and piecewise constants c_1, c_2 , minimize (??) with respect to bias field estimator B .
- b) For fixed characteristic function χ_1, χ_2 and bias field estimator B , minimize (??) with respect to piecewise constants c_1, c_2 .

- c) For fixed piecewise constants c_1, c_2 and bias field estimator B , minimize (??) with respect to characteristic function χ_1, χ_2 .

In the following subsection, we will present the solutions for the three optimization steps.

C. Gaussian Kernel-based Bias Field Estimator

Inspired by the regularization theory of Nielsen et al. [?] that linear convolution of a signal can be the exact minimizer for certain energy functionals related to this signal, we give the following minimization method for the energy minimization step a) with respect to the bias field estimator B , which is shown in Proposition 1.

Proposition 1: Suppose that ι_1 and ι_2 are characteristic functions of one-dimension intervals τ_1 and τ_2 respectively, where $\iota_1 = 1 - \iota_2$ and $\tau_1 = \tau - \tau_2$. For any given constants c_1, c_2 and characteristic functions ι_1 and ι_2 , the following energy:

$$\begin{aligned} \xi = & \lambda \int_{\tau} ((S - Bc_1)^2 \iota_1 + (S - Bc_2)^2 \iota_2) dx \\ & + \int_{\tau} \sum_{k=1}^{+\infty} \mu_k \left(\frac{\partial^k B}{\partial x^k} \right)^2 dx \end{aligned} \quad (10)$$

can be solved by one of the following convolutions:

$$B = \frac{(c_1 S(x) \iota_1(x)) * g_{\sigma_1} + (c_2 S(x) \iota_2(x)) * g_{\sigma_2}}{c_1^2 \iota_1 + c_2^2 \iota_2} \quad (11)$$

or

$$B = \frac{(S(x) \iota_1(x)) * g_{\sigma_1} + (S(x) \iota_2(x)) * g_{\sigma_2}}{c_1 \iota_1 + c_2 \iota_2} \quad (12)$$

where $u_k = \frac{\eta^k}{k!}$ is a weighting constant. S, B are one-dimension signals in τ and $g_{\sigma_1}, g_{\sigma_2}$ are two Gaussian kernel functions with standard deviations σ_1 and σ_2 respectively. The operator " * " means convolution.

Proof: For convenience, we recall the energy ξ in (??) as follows:

$$\begin{aligned} \xi = & \lambda \int_{\tau} ((S - Bc_1)^2 \iota_1 + (S - Bc_2)^2 \iota_2) dx \\ & + \int_{\tau} \sum_{k=1}^{+\infty} \mu_k \left(\frac{\partial^k B}{\partial x^k} \right)^2 dx \end{aligned} \quad (13)$$

Obviously, formulation (??) is equivalent to the following equation:

$$\begin{aligned}\xi_1 = & \lambda \int_{\tau} ((S \cdot \iota_1 - B \cdot \iota_1 \cdot c_1)^2 + (S \cdot \iota_2 - B \cdot \iota_2 \cdot c_2)^2) dx \\ & + \int_{\tau} \sum_{k=1}^{+\infty} \mu_k \left(\frac{\partial^k B}{\partial x^k} \cdot (\iota_1 + \iota_2) \right)^2 dx\end{aligned}\quad (14)$$

Since ι_1 and ι_2 are characteristic functions and $(\iota_1 + \iota_2) = 1$, we have:

$$(\iota_1 + \iota_2)^2 = \iota_1^2 + \iota_2^2 \quad (15)$$

Thereby, we rewrite (??) integrating with (??) as follows:

$$\begin{aligned}\xi_2 = & \lambda \int_{\tau} ((S \iota_1 - B \iota_1 c_1)^2 + (S \iota_2 - B \iota_2 c_2)^2) dx \\ & + \int_{\tau} \sum_{k=1}^{+\infty} \mu_k \left(\left(\frac{\partial^k B}{\partial x^k} \iota_1 \right)^2 + \left(\frac{\partial^k B}{\partial x^k} \iota_2 \right)^2 \right) dx\end{aligned}\quad (16)$$

According to Parsevals Theorem, transforming energy ξ_2 to the Fourier domain [?] will yield the following energy:

$$\begin{aligned}\widehat{\xi}_2 = & \lambda \int ((\widehat{S} * \widehat{\iota}_1 - \widehat{B} * \widehat{\iota}_1 c_1)^2 + (\widehat{S} * \widehat{\iota}_2 - \widehat{B} * \widehat{\iota}_2 c_2)^2) d\omega \\ & + \int \sum_{k=1}^{+\infty} \mu_k \omega^{2k} ((\widehat{B} * \widehat{\iota}_1)^2 + (\widehat{B} * \widehat{\iota}_2)^2) d\omega\end{aligned}\quad (17)$$

where $\widehat{\xi}_2, \widehat{S}, \widehat{\iota}_1$ and $\widehat{\iota}_2$ are the Fourier transformation of ξ_2, S, ι_1 and ι_2 , respectively. Keeping c_1, c_2 and ι_1, ι_2 fixed, computing the related Euler-Lagrange equation for $\widehat{\xi}_2$ with respect to \widehat{B} yields the following partial differential equation:

$$\begin{aligned}\frac{\partial \widehat{\xi}_2}{\partial \widehat{B}} = & \lambda c_1 (\widehat{B} * \widehat{\iota}_1 c_1 - \widehat{S} * \widehat{\iota}_1) \cdot (1 * \widehat{\iota}_1) \\ & + \lambda c_2 (\widehat{B} * \widehat{\iota}_2 c_2 - \widehat{S} * \widehat{\iota}_2) \cdot (1 * \widehat{\iota}_2) \\ & + \sum_{k=1}^{+\infty} \mu_k \omega^{2k} \cdot (\widehat{B} * \widehat{\iota}_1) \cdot (1 * \widehat{\iota}_1) \\ & + \sum_{k=1}^{+\infty} \mu_k \omega^{2k} \cdot (\widehat{B} * \widehat{\iota}_2) \cdot (1 * \widehat{\iota}_2)\end{aligned}\quad (18)$$

A sufficient and necessary condition for energy $\hat{\xi}_2$ to achieve its minimum is that $\frac{\partial \hat{\xi}_2}{\partial \hat{B}} \equiv 0$, i.e., we have

$$\begin{aligned}
& c_1(\hat{B} * \hat{t}_1 c_1 - \hat{S} * \hat{t}_1)(1 * \hat{t}_1) + c_2(\hat{B} * \hat{t}_2 c_2 - \hat{S} * \hat{t}_2)(1 * \hat{t}_2) \\
& + \sum_{k=1}^{+\infty} \frac{\mu_k}{\lambda} \omega^{2k} (\hat{B} * \hat{t}_1)(1 * \hat{t}_1) + \sum_{k=1}^{+\infty} \frac{\mu_k}{\lambda} \omega^{2k} (\hat{B} * \hat{t}_2)(1 * \hat{t}_2) \\
& \equiv 0
\end{aligned} \tag{19}$$

\Leftrightarrow

$$\begin{aligned}
& \underbrace{c_1 \hat{S} * \hat{t}_1 \cdot (1 * \hat{t}_1)}_{term1} + \underbrace{c_2 \hat{S} * \hat{t}_2 \cdot (1 * \hat{t}_2)}_{term2} = \\
& \underbrace{(c_1^2 (\hat{B} * \hat{t}_1) + \sum_{k=1}^{+\infty} \frac{\mu_k}{\lambda} \omega^{2k} (\hat{B} * \hat{t}_1)) (1 * \hat{t}_1)}_{term3} \\
& + \underbrace{(c_2^2 (\hat{B} * \hat{t}_2) + \sum_{k=1}^{+\infty} \frac{\mu_k}{\lambda} \omega^{2k} (\hat{B} * \hat{t}_2)) (1 * \hat{t}_2)}_{term4}
\end{aligned} \tag{20}$$

We can see that (??) can be solved by making $term1 = term3$ and $term2 = term4$, i.e., (??) can be solved by the following equations:

$$c_1 \hat{S} * \hat{t}_1 = c_1^2 (\hat{B} * \hat{t}_1) \left(1 + \sum_{k=1}^{+\infty} \mu_k \frac{\omega^{2k}}{c_1^2} (\hat{B} * \hat{t}_1)\right) \tag{21a}$$

$$c_2 \hat{S} * \hat{t}_2 = c_2^2 (\hat{B} * \hat{t}_2) \left(1 + \sum_{k=1}^{+\infty} \mu_k \frac{\omega^{2k}}{c_2^2} (\hat{B} * \hat{t}_2)\right) \tag{21b}$$

In (??), since $u_k = \frac{\eta^k}{k!}$, we have

$$\begin{aligned}
& 1 + \sum_{k=1}^{+\infty} \mu_k \frac{\omega^{2k}}{c_1^2} = 1 + \sum_{k=1}^{+\infty} \frac{(\lambda^{\frac{1}{-k}} c_1^{-\frac{2}{k}} \eta)^k}{k!} \omega^{2k} \\
& = \exp(-\lambda^{\frac{1}{-k}} c_1^{-\frac{2}{k}} \eta \omega)
\end{aligned} \tag{22a}$$

$$\begin{aligned}
& 1 + \sum_{k=1}^{+\infty} \mu_k \frac{\omega^{2k}}{c_2^2} = 1 + \sum_{k=1}^{+\infty} \frac{(\lambda^{\frac{1}{-k}} c_2^{-\frac{2}{k}} \eta)^k}{k!} \omega^{2k} \\
& = \exp(-\lambda^{\frac{1}{-k}} c_2^{-\frac{2}{k}} \eta \omega)
\end{aligned} \tag{22b}$$

Let $\hat{g}_{\sigma_1} = \exp(-\lambda^{\frac{1}{-k}} c_1^{-\frac{2}{k}} \eta \omega)$ and $\hat{g}_{\sigma_2} = \exp(-\lambda^{\frac{1}{-k}} c_2^{-\frac{2}{k}} \eta \omega)$. It is obvious that \hat{g}_{σ_1} and \hat{g}_{σ_2} are two Gaussian kernel functions with standard deviations $\sigma_1 = \sqrt{2\lambda^{\frac{1}{-k}} c_1^{-\frac{2}{k}} \eta}$ and $\sigma_2 = \sqrt{2\lambda^{\frac{1}{-k}} c_2^{-\frac{2}{k}} \eta}$ respectively. By adding (21a) to (21b), we can obtain that

$$c_1 \hat{S} * \hat{t}_1 + c_2 \hat{S} * \hat{t}_2 = c_1^2 (\hat{B} * \hat{t}_1) \hat{g}_{\sigma_1} + c_2^2 (\hat{B} * \hat{t}_2) \hat{g}_{\sigma_2} \quad (23)$$

or

$$\hat{S} * \hat{t}_1 + \hat{S} * \hat{t}_2 = c_1 (\hat{B} * \hat{t}_1) \hat{g}_{\sigma_1} + c_2 (\hat{B} * \hat{t}_2) \hat{g}_{\sigma_2} \quad (24)$$

Transforming (??) and (??) into spatial domain will yield

$$B = \frac{(c_1 S(x) t_1(x)) * g_{\sigma_1} + (c_2 S(x) t_2(x)) * g_{\sigma_2}}{c_1^2 t_1 + c_2^2 t_2} \quad (25)$$

or

$$B = \frac{(S(x) t_1(x)) * g_{\sigma_1} + (S(x) t_2(x)) * g_{\sigma_2}}{c_1 t_1 + c_2 t_2} \quad (26)$$

■

Since Gaussian kernel function is Cartesian invariants, according to the theory by Nielsen et al. [?] and analysis by Brox [?], (??) and (??) can be directly generalized to higher dimensions. Thereby, the convolution

$$B = \frac{c_1 \chi_1(x) * G_{\sigma_1} + c_2 \chi_2(x) * G_{\sigma_2}}{c_1^2 \chi_1 + c_2^2 \chi_2} I(x) \quad (27)$$

will be an exact minimizer of

$$\begin{aligned} E_0 = & \lambda \int_{\Omega} ((I - Bc_1)^2 \chi_1 + (I - Bc_2)^2 \chi_2) dx dy \\ & + \int_{\Omega} \sum_{i+j=k}^{+\infty} \mu_k \left(\frac{\partial^k B}{\partial x^i \partial y^j} \right)^2 dx dy + \nu |C| \end{aligned} \quad (28)$$

Ignoring all bias field estimator smoothness penalizer terms for of order $k > 1$ may yield

$$\begin{aligned} E_1 = & \lambda \int_{\Omega} ((I - Bc_1)^2 \chi_1 + (I - Bc_2)^2 \chi_2) dx dy \\ & + \mu \int_{\Omega} |\nabla B|^2 dx dy + \nu |C| \end{aligned} \quad (29)$$

In our work, (??) can be well approximated by

$$B = \frac{c_1 I \chi_1 + c_2 I \chi_2}{c_1^2 \chi_1 + c_2^2 \chi_2} * G \quad (30)$$

where G is a Gaussian. The convolution shown in (??) may ensure the bias field estimator B keep smooth in the whole image domain.

For the energy minimization step b), given the fixed χ_1 , χ_2 and B , the minimum of (??) with respect to fitting constants c_1 , c_2 can be achieved by computing the corresponding Euler-Lagrange equation:

$$\begin{aligned} \frac{\partial E_1}{\partial c_1} &= \int_{\Omega} (I(x) - B c_1) B \chi_1 dx = 0 \\ \frac{\partial E_1}{\partial c_2} &= \int_{\Omega} (I(x) - B c_2) B \chi_2 dx = 0 \end{aligned} \quad (31)$$

\Rightarrow

$$c_1 = \frac{\int_{\Omega} I(x) B(x) \chi_1 dx}{\int_{\Omega} B^2(x) \chi_1 dx}, \quad c_2 = \frac{\int_{\Omega} I(x) B(x) \chi_2 dx}{\int_{\Omega} B^2(x) \chi_2 dx} \quad (32)$$

D. Global Minimum

As discussed in [?], one of the main drawbacks of traditional active contour models is that they cannot find the global minima. As χ_1 and χ_2 take only the values 1 and 0, the proposed energy (??) cannot find the global minimum with respect to χ_1 and χ_2 , i.e. the following minimization problem can only find the non-global minimum with respect to Ω_1 (where Ω_1 is the image domain outside the active curves.):

$$\begin{aligned} \min_{\chi_1, \chi_2} \{ E_2 = & \lambda \int_{\Omega} ((I - B c_1)^2 \chi_1 + (I - B c_2)^2 \chi_2) dx \\ & + \nu |C| \} \end{aligned} \quad (33)$$

In this paper, based on the new variational framework of T.Chan et al. [?] and Bresson et al. [?], we propose to find the energy shown in (??) by solving the following minimization problem:

$$\begin{aligned} \min_{0 \leq u \leq 1} \{E_3 &= \lambda \int_{\Omega} (I - Bc_1)^2 u dx + \lambda \int_{\Omega} (I - Bc_2)^2 (1 - u) dx \\ &+ \nu \int_{\Omega} |\nabla u|^2 dx\} \end{aligned} \quad (34)$$

In (??), the characteristic functions χ_1 and χ_2 are replaced by u and $1 - u$ where $0 \leq u \leq 1$, which means that the minimization problem of (??) over the non-convex set $\{\chi_1\}$ (or $\{\chi_2\}$) has been extended to the convex set $\{u \in BV(\Omega), 0 \leq u \leq 1\}$, just as discussed by [?]. Thereby, we can find the global minimum of (??) with respect to u . The following theory will give the relationship between the optimization problem of (??) and (??).

Theorem 1: Suppose that $I(x) \in [0, 1]$. For any given c_1, c_2 and B , if $u(x)$ is any minimizer of $E_3(c_1, c_2, B, \cdot)$, then for almost every $\varepsilon \in [0, 1]$, the characteristic function $\mathbf{1}_{\{x:u(x)>\varepsilon\}}$ is a global minimizer of $E_1(c_1, c_2, B, \cdot)$.

Proof: Inspired by the proof formulated in [?], [?], [?], and according to the coarea formula, we rewrite the energy E_3 :

$$\begin{aligned} E_3(u, c_1, c_2, B) &= \lambda \int_{\Omega} (I - Bc_1)^2 u dx + \lambda \int_{\Omega} (I - Bc_2)^2 \times \\ &(1 - u) dx + \nu \int_{\Omega} |\nabla u|^2 dx \\ &= \lambda \int_{\Omega} (I - Bc_1)^2 \int_0^1 \mathbf{1}_{[0, u(x)]}(\varepsilon) d\varepsilon dx + \lambda \int_{\Omega} (I - Bc_2)^2 \times \\ &\int_0^1 \mathbf{1}_{[u(x), 1]}(\varepsilon) d\varepsilon dx + \nu \int_{\Omega} |\nabla u|^2 dx \end{aligned} \quad (35)$$

Let $D = \{x : u(x) > \varepsilon\}$ and rewrite (??) integrating with set D :

$$\begin{aligned} E_3(u, c_1, c_2, B) &= \lambda \int_{\Omega} (I - Bc_1)^2 \int_0^1 \mathbf{1}_{[0, u(x)]}(\varepsilon) d\varepsilon dx \\ &+ \lambda \int_{\Omega} (I - Bc_2)^2 \int_0^1 \mathbf{1}_{[u(x), 1]}(\varepsilon) d\varepsilon dx + \nu \int_0^1 \text{Per}(D(\varepsilon)) d\varepsilon \end{aligned} \quad (36)$$

Moving the integral over x inside the integral over ε , we can obtain

$$\begin{aligned} E_3(u, c_1, c_2, B) &= \int_0^1 \left\{ \lambda \int_{\Omega} ((I - Bc_1)^2 \mathbf{1}_{[0, u(x)]} \right. \\ &+ (I - Bc_2)^2 \mathbf{1}_{[u(x), 1]}) dx + \nu \text{Per}(D(\varepsilon)) \left. \right\} d\varepsilon \\ &= \int_0^1 E_2(D, c_1, c_2, B) d\varepsilon \end{aligned} \quad (37)$$

It means that if $u(x)$ is a global minimizer of E_3 , then for almost every $\varepsilon \in [0, 1]$, the set $D(\varepsilon)$ is a global minimizer of minimization problem (??). ■

For convenience, we denote the total variation $\int_{\Omega} |\nabla u| dx$ in (??) by $\text{TV}(u)$. Then the minimization problem of (??) with respect to u can be efficiently solved by the dual formulation method [?], [?]. Thereby, we solve the following minimization problem by adding a new variable v :

$$\begin{aligned} \min_{u,v} \{ & E_4 = \nu \text{TV}(u) + \frac{1}{2\theta} \int_{\Omega} (u(x) - v(x))^2 dx \\ & + \int_{\Omega} \lambda r(x, c_1, c_2) + \alpha \psi(u) dx \} \end{aligned} \quad (38)$$

where $r(x, c_1, c_2) = (I - Bc_1)^2 - (I - Bc_2)^2$ and $\theta > 0$ is a small parameter. $\alpha \psi(u)$ is an exact penalty term [?] used to extend the constrained convex set $\{u \in BV(\Omega), 0 \leq u \leq 1\}$ to unconstrained convex set $\{u \in BV(\Omega)\}$, where $\psi(u) = \max\{0, 2|u - \frac{1}{2}| - 1\}$, provided that $\alpha > \frac{\lambda}{2} \|r(x, c_1, c_2)\|_{L^\infty(\Omega)}$.

The minimization of (??) for given c_1, c_2 and B can be solved iteratively by the following two steps:

(i) v being fixed, minimize the following functional F_1 with respect to u :

$$F_1(u) = \text{TV}(u) + \frac{1}{2\theta} \|u(x) - v(x)\|_{L^2}^2 \quad (39)$$

(ii) u being fixed, minimize the following functional F_2 with respect to v :

$$\begin{aligned} F_2(v) = & \frac{1}{2\theta} \|u(x) - v(x)\|_{L^2}^2 + \int_{\Omega} \lambda r(x, c_1, c_2) v \\ & + \alpha \psi(v) dx \end{aligned} \quad (40)$$

Following Chambolle's dual formulation method [?], the step (i) can be efficiently solved by:

$$u(x) = v(x) - \theta \text{div} \rho(x) \quad (41)$$

where $\rho = (\rho^1, \rho^2)$ is the solution of

$$\nabla(\theta \text{div} \rho - v) - |\nabla(\theta \text{div} \rho - v)| \rho = 0 \quad (42)$$

(??) can be solved by a fixed point method $\rho^0 = 0$ and

$$\rho^{n+1} = \frac{\rho^n + \delta_t \nabla(\operatorname{div}(\rho^n) - v/\theta)}{1 + \delta_t |\operatorname{div} \rho^n - v/\theta|} \quad (43)$$

The solution of (??) is achieved by the method of [?]:

$$v(x) = \min\{\max\{u(x) - \theta \lambda r(x, c_1, c_2), 0\}, 1\} \quad (44)$$

E. Numerical Implementation

In this paper, we compute the fitting constants shown in (??) by the smooth region descriptors $H_\zeta^{(1)}$ and $H_\zeta^{(2)}$ instead of the characteristic functions χ_1 and χ_2 . The smooth region descriptors $H_\zeta^{(1)}$ and $H_\zeta^{(2)}$ where $H_\zeta^{(1)} = 1 - H_\zeta^{(2)}$ can be described as:

$$H_\zeta^{(1)}(\varphi(x)) = \frac{1}{2} \left(1 + \frac{2}{\pi} \arctan(\varphi * G_\zeta) \right), \quad x \in \Omega \quad (45)$$

where G_ζ is a Gaussian kernel and ζ is standard deviation. From (??) we can see that $H_\zeta^{(1)}$ is rather similar to the regularized version of Heaviside function introduced by [?]. Variable $\varphi(x)$ is computed in terms of u :

$$\varphi(x) = \begin{cases} c, & \text{for } x \in \Omega: u(x) > \varepsilon \\ -c, & \text{for } x \in \Omega: u(x) \leq \varepsilon \end{cases} \quad (46)$$

where $\varepsilon \in [0, 1]$ and $c > 0$ are two given constants. The convolution $\phi = \varphi * G_\zeta$ in (??) is to ensure the value of ϕ to be small around the curves C and keep smooth in Ω . Thus the region descriptor $H_\zeta^{(1)}$ can be smooth. Based on the region descriptors $H_\zeta^{(1)}$ and $H_\zeta^{(2)}$, the fitting constants c_1 and c_2 can be computed by:

$$c_1 = \frac{\int_\Omega I(x) B(x) H_\zeta^{(1)} dx}{\int_\Omega B^2(x) H_\zeta^{(1)} dx}, c_2 = \frac{\int_\Omega I(x) B(x) H_\zeta^{(2)} dx}{\int_\Omega B^2(x) H_\zeta^{(2)} dx} \quad (47)$$

In this paper, we choose $c = 2, \zeta = 1$ for each experiment. The curve-length weighting parameter ν and time step δ_t can be set as $\nu = 1$ and $\delta_t = 1/8$. We also set $\theta = 1/3$ for all experiments. The standard

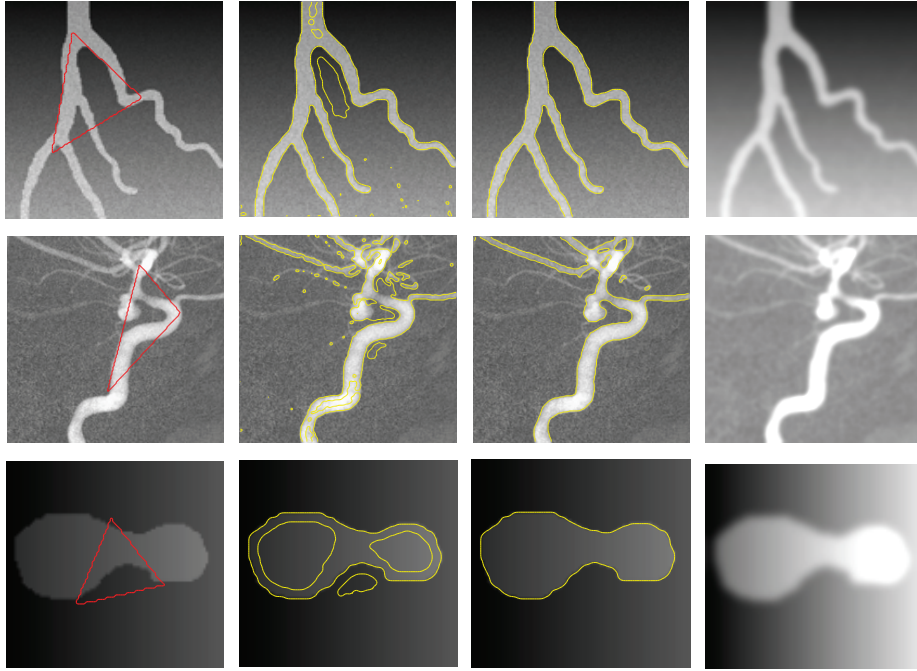


Fig. 1. Segmentation results of our method with $\lambda = 0.006 \times 255^2$, $\varepsilon = 0.5$ and $\sigma = 3$. Columns 1 to 4 are initial curves, intermediate results, final results and bias field estimation respectively.

deviation σ of Gaussian kernel in (??), the weighting parameter λ in (??) and constant $\varepsilon \in [0, 1]$ will be related to each experimental image. Also, The Gaussian kernel can be truncated as a mask with size $\varrho \times \varrho$ (ϱ is the the smallest odd number following that $\varrho \geq 4\sigma + 1$ where σ is the standard deviation of Gaussian kernel [?]). Unless otherwise specified, we update the u and v for each iteration and update c_1 , c_2 and B for every two iterations.

IV. EXPERIMENTAL RESULTS

In the following experiments, we perform our Matlab codes on a PC with Pentium dual-core E5400 processor, 2.70 GHz, 2GB RAM.

A. Performance Evaluation

In this section, we test our method both in synthetic and medical images especially for vessel images. Firstly, we demonstrate the performance of our method in two vessel images and a synthetic image as shown in Fig. 1. Curve evolution process including the initial curves, intermediate results and final results

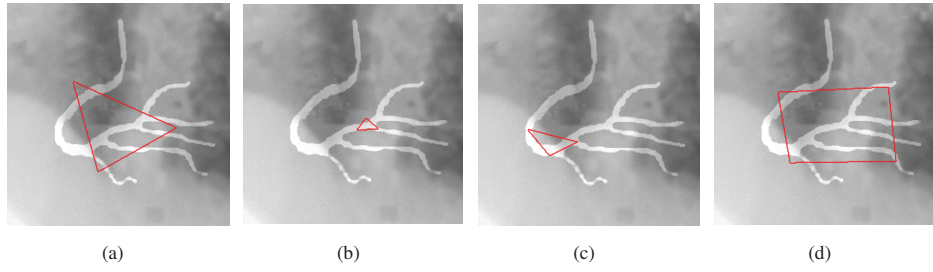


Fig. 2. Different initializations for synthetic images with size 256×256 .

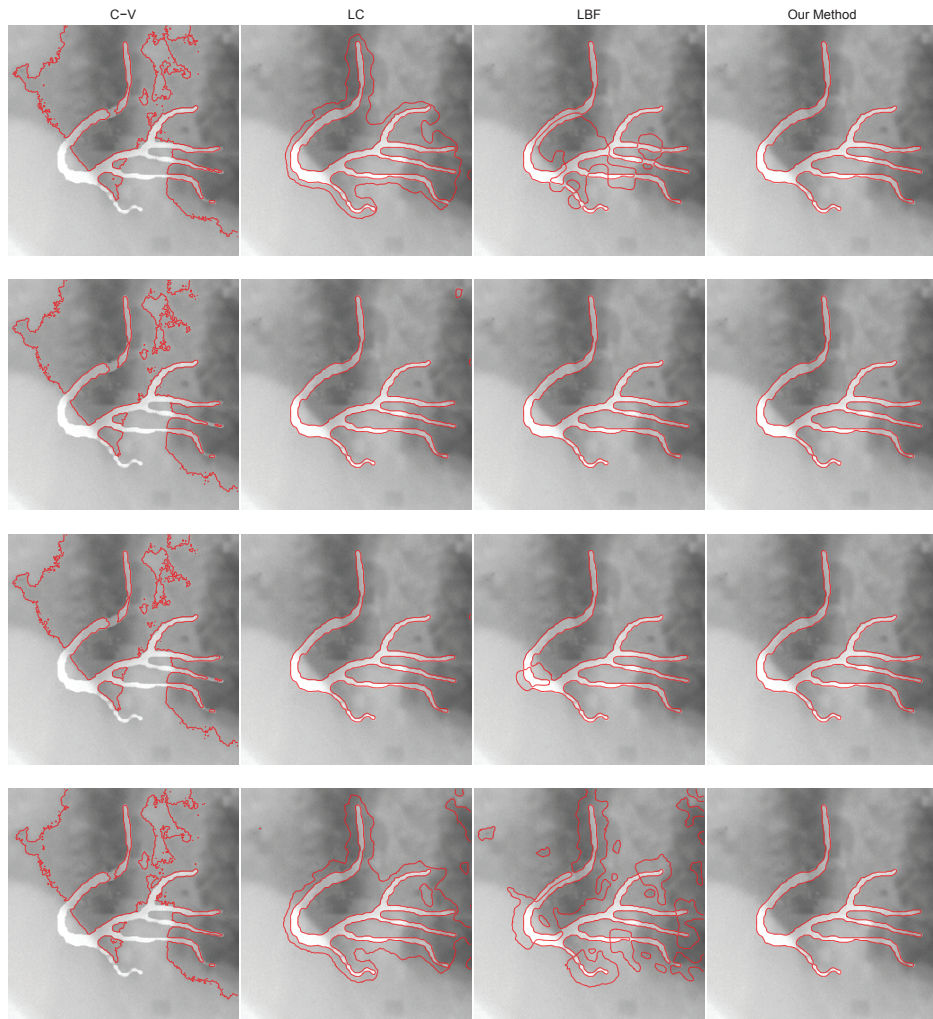


Fig. 3. Segmentation results for synthetic images. Rows 1 to 4 are the segmentation results with initializations corresponding to Fig.2 (a) to (d) respectively.

are plotted on images in columns 1 to 3. Column 4 shows the bias field estimator. Though intensity inhomogeneities of the three images shown in Fig. 1 are rather obvious, the performance of our method

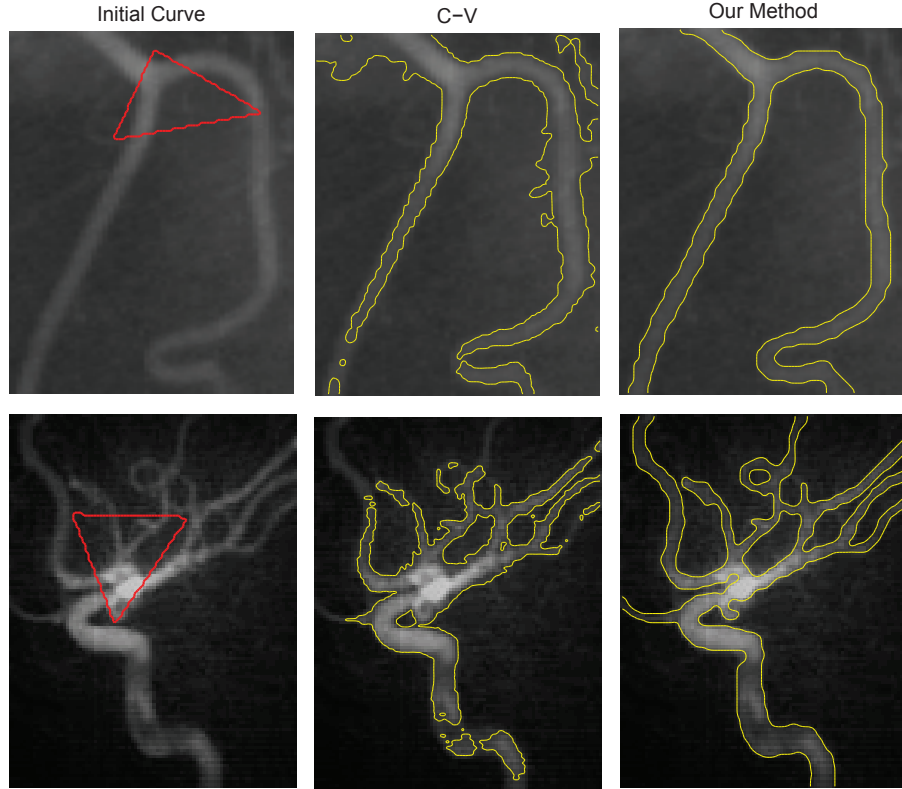


Fig. 4. Performances of C-V model and our model for two vessel images. The left, middle and right columns are initial curves, results by C-V model and results by our model respectively.

can achieve desire results. Furthermore, from column 4 of Fig. 1, we can see that the bias field estimator computed by (??) can keep smooth in the whole image domain just as discussed in section III.

Let C_t denote the ground truth contours and P_i denote the i^{th} pixel located at the detected curves. In order to evaluate our method, we perform the following metric:

$$e_{min} = \frac{1}{N} \sum_{i=1}^N \text{Dis}(C_t, P_i) \quad (48)$$

where $\text{Dis}(C_t, P_i)$ is the minimal distance among all the distances from pixel P_i to each pixel of C_t . N is the total number of pixels on the detected contours. This metric can evaluate the segmentation results with subpixel accuracy.

Fig. 2 shows four different initializations on the same synthetic image with tubular tree structure as

the object. As the ground truth contours of Fig. 2 have been known, we make use of Fig. 2 to evaluate the performance of the C-V model [?] , LBF model [?] and LC model [?] as well as our method. Fig. 3 demonstrates the segmentation results for the three methods and our method respectively. For our method in Fig. 3, we update the u and v for each iteration and update c_1 , c_2 and B for every four iterations.

The C-V model utilizes only two fitting constants to approximate the image inside and outside the curves, which will lead to false results. Column 1 of Fig. 3 demonstrate the performance of C-V model and many false curves are detected under any initializations. Column 2 shows the segmentation results by LC method which is able to handle under intensity inhomogeneities. However, due to the level set application, under some initializations, LC model may suffer from local minimums. LBF model makes use of local binary fitting data to approximate the image in a local region. This method is robust to intensity inhomogeneities but will introduce amounts of local minimums. Column 3 shows the results by LBF model. Under the initializations shown in Fig. 2(c), LBF can obtain good results. However, under the other initializations it will result false segmentation curves. Columns 4 demonstrates the results of our method with $\lambda = 0.015 \times 255^2$, $\sigma = 4$ and $\varepsilon = 0.5$. It can be seen that under different initializations, our method will result the same segmentation curves, i.e. our method is more robust against the initialization than LC model and LBF model. The mean computational time of our method in Fig. 3 is about 27 seconds.

Table 1 shows the quantitative evaluation results computed by (??). For four initializations, the evaluation results of our method are almost the same. The evaluation values of C-V model seem to be much higher than the other methods. And the results of LBF and LC are very similar, both of which are higher than our method.

In Fig. 4, we compare the C-V model and our model in two real vessel images with size 131×103 (the top row) and 122×94 (the bottom row). Notice that the C-V model can only identify regions with brightest intensity while our method can find the accurate partitions of the images. As both the background and foreground of the images shown in Fig. 4 vary smoothly and quickly, the image model formulated by piecewise constants used in C-V mode cannot work well. Instead, our model utilizing the piecewise smooth image model can handle the intensity inhomogeneities more accurately. The mean computational time of our method for Fig. 4 based on the parameters $\lambda = 0.005 \times 255^2$ ($\lambda = 0.01 \times 255^2$ for the bottom row), $\sigma = 4$ and $\varepsilon = 0.5$ is about 6.5 seconds.

TABLE I. QUANTITATIVE EVALUATION RESULTS OF DIFFERENT ACTIVE CONTOUR MODELS FOR IMAGES SHOWN IN FIG.3

Methods	Row 1	Row 2	Row 3	Row 4
C-V	19.6350	20.0497	20.0651	19.4441
LC	2.8336	2.7025	1.2405	7.2686
LBF	2.3486	1.0839	1.3529	11.1026
Our Method	1.0810	1.0816	1.0816	1.0810

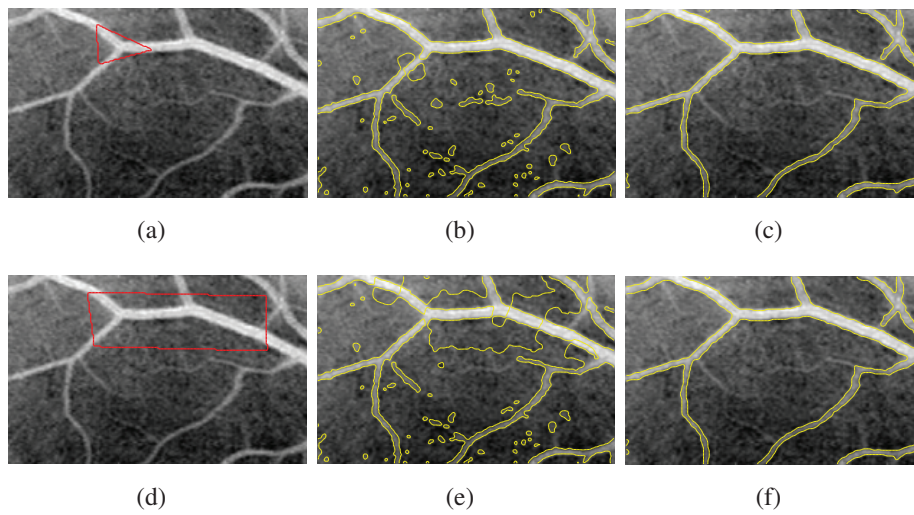


Fig. 5. Performances of LBF model and our model with different initializations. (a) and (d) are two different initializations. (b) and (e) are segmentation results of LBF model. (c) and (f) are segmentation results of our model with $\lambda = 0.0037 \times 255^2$, $\sigma = 3$ and $\varepsilon = 0.45$.

Fig. 5, Fig. 6 and Fig. 7 are the comparison of performance between LBF model and our model for clinic images with two different initializations for each image. Fig. 5(b) and (e) are the results by LBF model which suffers from many local minima especially around the initial curve. Fig. 5(c) and (f) are the segmentation results by our model and can capture the accurate contour. Fig. 6 and Fig. 7 share the same explanation with Fig. 5. Compared to LBF model, our method can avoid suffering from the local minima due to the new variational framework [?] to find the global minimum and the two constants in(??) to give our model a global restriction. The mean computational time of our method for Fig. 5 with size 131×207 , Fig. 6 with size 110×111 and Fig. 7 with size 151×151 are about 18.3, 11.3 and 27.3 seconds, respectively.

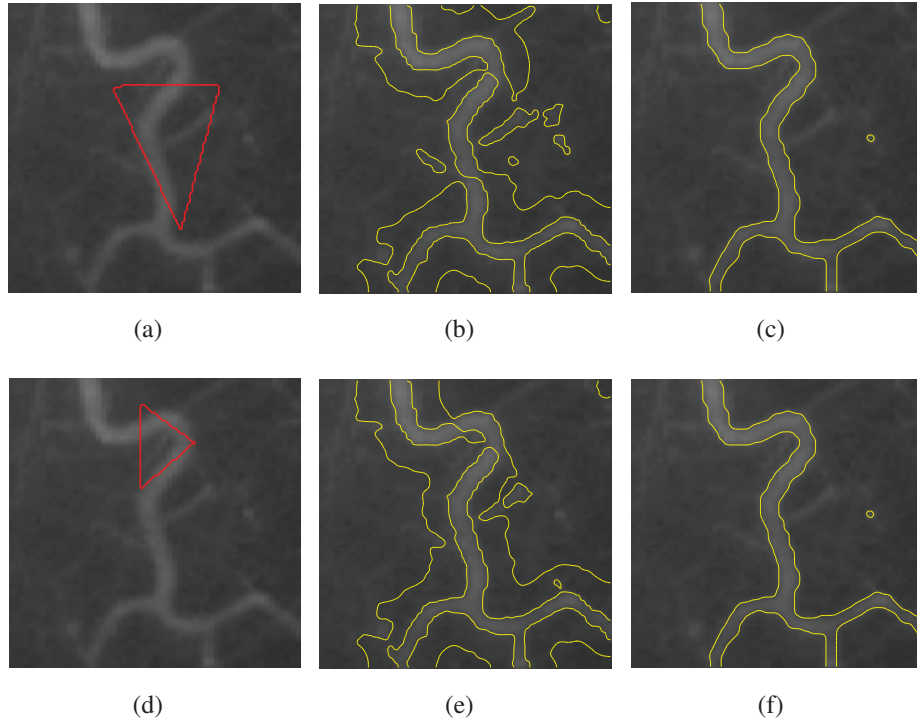


Fig. 6. Performances of LBF model and our model with different initializations. (a) and (d) are two different initializations. (b) and (e) are segmentation results of LBF model. (c) and (f) are segmentation results of our model with $\lambda = 0.08 \times 255^2$, $\sigma = 3$ and $\varepsilon = 0.45$.

In the next examples (Figs. 8, 9 and 10) we compare the LC model based on level set formulation with our method. Fig. 8 shows the performance of LC model and our model in a 138×137 -size vessel image with weak edges. Fig. 8(a) is the initial curve, Fig. 8(b) is the result by LC model and Fig. 8(c) is the result by our method. The LC model based on level set formulation and local cluster finds a large amount of false curves while our model can capture the main tubular structure. It costs about 19.3 seconds for our method to guide the curves to convergence to the boundaries in Fig. 8. Fig. 9 shows the segmentation results of LC model and our method for a ultrasound image with weak edges as well and shares the same instruction with Fig. 8. It will take about 20 seconds for our method to segment Fig. 9 with size 202×249 . The original image in Fig. 10(a) and (d) is the same one as shown in Fig. 5. With two different initializations as shown in Fig. 10(a) and (d), we demonstrate the performance of LC model and our model. Similar to the segmentation results of LBF in Fig. 5(b) and (d), Fig. 10(b) and (d) also suffer from the local minima especially around the initial curve.

Fig. 11 shows the segmentation results by LC model with different curve-length parameters (denoted by

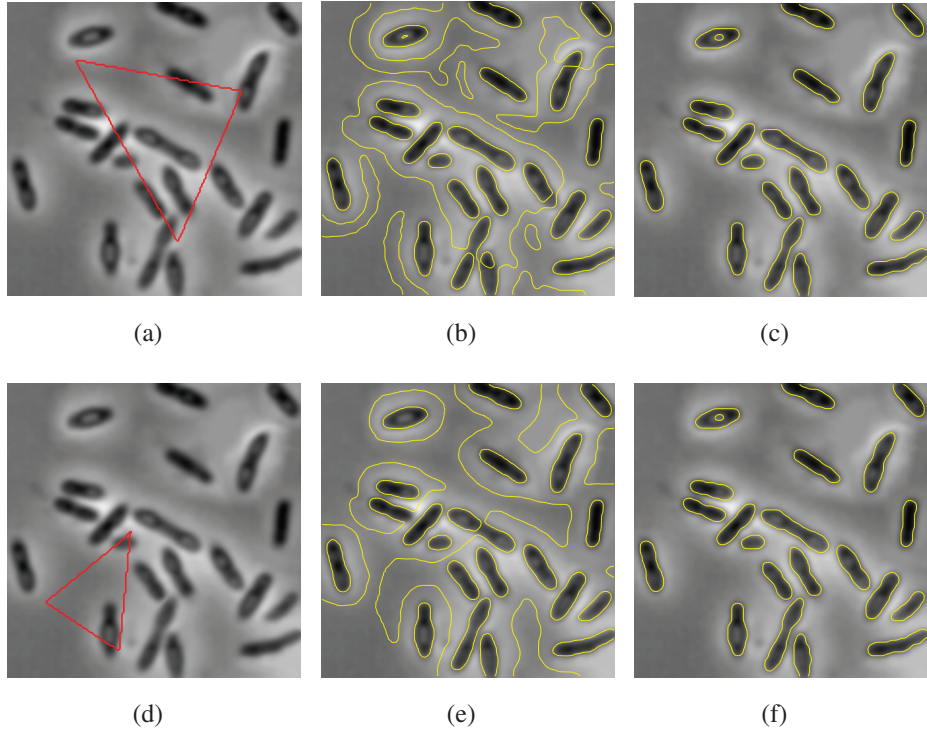


Fig. 7. Segmentation results of LBF model and our model with different initializations. (a) and (d) are two different initializations. (b) and (e) are segmentation results of LBF model. (c) and (f) are segmentation results of our model with $\lambda = 0.007 \times 255^2$, $\sigma = 3$ and $\varepsilon = 0.65$.

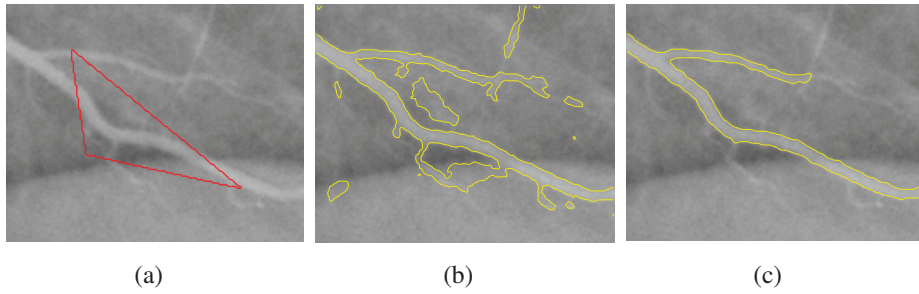


Fig. 8. Segmentation results of LC model and our method. (a) is initial curve. (b) is the performance of LC model. (c) is the performance of our model with $\lambda = 0.017 \times 255^2$, $\sigma = 4$ and $\varepsilon = 0.45$.

ν). The initialization for Fig. 11 is the same as in Fig.10(d). It can be seen that the LC model falls into local minima around the initial curve though we give more weight to curve-length energy.

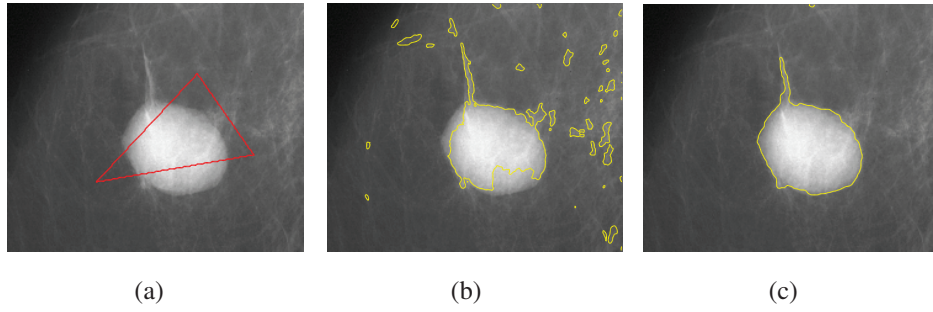


Fig. 9. Segmentation results of LC model and our method for ultrasound image. (a) is initial curve. (b) is the performance of LC model. (c) is the performance of our model with $\lambda = 0.035 \times 255^2$, $\sigma = 4$ and $\varepsilon = 0.45$.

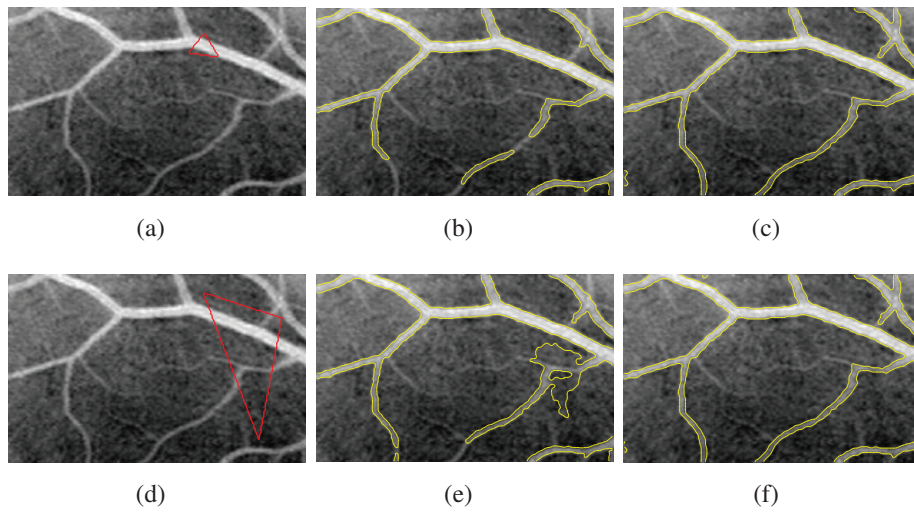


Fig. 10. Performances of LC model and our model with different initializations. (a) and (d) are two different initializations. (b) and (e) are segmentation results of LC model. (c) and (f) are segmentation results of our model with $\lambda = 0.0035 \times 255^2$, $\sigma = 3$ and $\varepsilon = 0.5$.

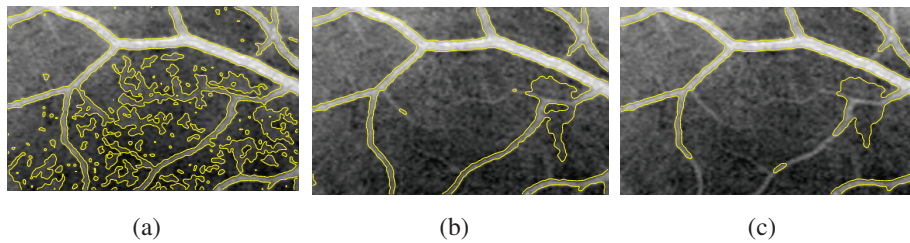


Fig. 11. Segmentation results of LC mode with different curve-length parameters ν . (a) results by setting $\nu = 0.001 \times 255^2$. (b) results by setting $\nu = 0.008 \times 255^2$. (c) results by setting $\nu = 0.015 \times 255^2$.

V. CONCLUSION

In this paper, we have presented a global active contour model with the bias field estimator for tubular structure segmentation. The proposed method can find the global minimum of the energy functional through the application of Chan's new variational framework and it is very robust against the initialization including shapes and positions. Also, Because of the existence of bias field estimator, our model is able to segment images with intensity inhomogeneities. Furthermore, we proposed a new method based on the Gaussian kernel function to calculate the bias field estimator, which can ensure the bias field estimator vary smoothly in image domain. Finally, by application of dual projection method and Bresson's work [?], our method can extract the boundaries more accurately than the widely used methods based on level set formulation like C-V model , LBF model and LC model. Meanwhile, experimental results on tubular and tree structure images further demonstrate the utility of the proposed method.

ACKNOWLEDGMENT

This work was supported by Excellent Youth and Middle Age Scientists Fund of Shandong Province(BS2010DX01) and Scientific Research Foundation for Returned Researcher of Ministry of Education of China.

REFERENCES

- [1] C. A. Davatzikos and J. L. Prince, "An active contour model for mapping the cortex," *IEEE Transactions on Medical Imaging*, vol. 14, no. 1, pp. 65–80, 1995.
- [2] C. Li, Z. D. Rui Huang, J. C. Gatenby, D. N. Metaxas, and J. C. Gore, "A level set method for image segmentation in the presence of intensity inhomogeneities with application to MRI," *IEEE Transactions on Image Processing*, vol. 20, no. 7, pp. 2007–2016, 2011.
- [3] M. Kass, A. Witkin, and D. Terzopoulos, "Snakes: Active contour models," *International journal of computer Vision*, vol. 1, no. 4, pp. 321–331, 1988.
- [4] L. D. Cohen, "On active contour models and balloons," *CVGIP: Image Understanding*, vol. 53, no. 2, pp. 211–218, 1991.
- [5] L. D. Cohen and I. Cohen, "Finite-element methods for active contour models and balloons for 2-D and 3-D images," *IEEE Transactions on Pattern Analysis and Machine Intelligence*, vol. 15, no. 11, pp. 1131–1147, 1993.
- [6] Kichenassamy, S. and Kumar, A. and Olver, P. and Tannenbaum, A. and Yezzi, A., "Gradient flows and geometric active contour models," *International Conference on Computer Vision*, pp.810–815, 1995.
- [7] Caselles V, Kimmel R and Sapiro G, "Geodesic active contours," *International Journal of Computer Vision*, vol. 22, no. 1, pp. 61–79, 1997.
- [8] S. Osher and J. A.Sethian, "Fronts propagating with curvature-dependent speed: Algorithms based on Hamilton-Jacobi formulations," *Journal of Computational Physics*, vol. 79, no. 1, pp. 12–49, 1988.

- [9] D. Mumford and J. Shah, "Optimal approximations by piecewise smooth functions and associated variational problems," *Communications on Pure and Applied Mathematics*, vol. 42, no. 5, pp. 577–685, 1989.
- [10] T. F. Chan and L. A. Vese, "Active contours without edges," *IEEE Transactions on Image Processing*, vol. 10, no. 2, pp. 266–277, 2001.
- [11] H. K. Zhao, T. Chan, B. Merriman, and S. Osher, "A variational level set approach to multiphase motion," *Journal of Computational Physics*, vol. 127, no. 1, pp. 179–195, 1996.
- [12] L. A. Vese and T. F. Chan, "A multiphase level set framework for image segmentation using the Mumford and Shah model," *International Journal of Computer Vision*, vol. 50, no. 3, pp. 271–293, 2002.
- [13] A. Tsai, A. Yezzi, and A. S. Willsky, "Curve evolution implementation of the Mumford-Shah functional for image segmentation, denoising, interpolation, and magnification," *IEEE Transactions on Image Processing*, vol. 10, no. 8, pp. 1169–1186, 2001.
- [14] C. Li, C.-Y. Kao, G. J. C., and Z. Ding, "Minimization of region-scalable fitting energy for image segmentation," *IEEE Transactions on Image Processing*, vol. 17, no. 10, pp. 1940–1949, 2008.
- [15] T. Brox and D. Cremers, "On local region models and a statistical interpretation of the piecewise smooth Mumford-Shah functional," *International Journal of Computer Vision*, vol. 84, no. 2, pp. 184–193, 2009.
- [16] S. Lankton and A. Tannenbaum, "Localizing region-based active contours," *IEEE Transactions on Image Processing*, vol. 17, no. 11, pp. 2029–2039, 2008.
- [17] M. Jung, G. Peyré, and L. D. Cohen, "Nonlocal Active Contours," *SIAM Journal on Imaging Sciences*, vol. 5, no. 3, pp. 1022–1054, 2012.
- [18] M. Jung, G. Peyré, and L. D. Cohen, "Non-local Active Contours," *Proc. SSVM11, Ein Gedi, Israel, 2011*.
- [19] L. Cohen and R. Kimmel, "Global minimum for active contour models: A minimal path approach," *International Journal of Computer Vision*, vol. 24, no. 1, pp. 57–78, 1997.
- [20] F. Benmansour and L. D. Cohen, "Fast object segmentation by growing minimal paths from a single point on 2D or 3D images," *Journal of Mathematical Imaging and Vision*, vol. 33, no. 2, pp. 209–221, 2009.
- [21] Chan TF, Esedoglu S and Nikolova M, "Algorithms for finding global minimizers of image segmentation and denoising models," *SIAM Journal on Applied Mathematics*, vol. 66, no. 5, pp. 1632–1648, 2006.
- [22] X. Bresson, S. Esedoglu, P. Vandergheynst, J.-P. Thiran, and S. Osher, "Fast global minimization of the active contour/snake model," *Journal of Mathematical Imaging and Vision*, vol. 28, no. 2, pp. 151–167, 2007.
- [23] A. Chambolle, "An algorithm for total variation minimization and applications," *Journal of Mathematical Imaging and Vision*, vol. 20, no. 1-2, pp. 89–97, 2004.
- [24] K. Sun, Z. Chen, and S. Jiang, "Local morphology fitting active contour for automatic vascular segmentation," *IEEE Transactions on Biomedical Engineering*, vol. 59, no. 2, pp. 464–473, 2012.
- [25] K. W. Sum and P. Y. S. Cheung, "Vessel extraction under non-uniform illumination: A level set approach," *IEEE Transactions on Biomedical Engineering*, vol. 55, no. 1, pp. 358–360, 2008.
- [26] F. Li, M. K. Ng, T. Y. Zeng, and C. Shen, "A multiphase image segmentation method based on fuzzy region competition," *SIAM Journal on Imaging Sciences*, vol. 3, no. 3, pp. 277–299, 2010.

- [27] F. Li, M. K. Ng, and C. Li, "Variational Fuzzy Mumford-Shah model for Image Segmentation," *SIAM Journal on Applied Mathematics*, vol. 70, no. 7, pp. 2750–2770, 2010.
- [28] D. L. Pham and J. L. Prince, "An adaptive fuzzy c-means algorithm for image segmentation in the presence of intensity inhomogeneities," *Pattern Recognition Letters*, vol. 20, no. 1, pp. 57–68, 1998.
- [29] M. N. Ahmed, S. M. Yamany, N. Mohamed, A. A. Farag, and T. Moriarty, "A modified fuzzy c-means algorithm for bias field estimation and segmentation of mri data," *IEEE Transactions on Medical Imaging*, vol. 21, no. 3, pp. 193–199, 2002.
- [30] D. L. Pham and J. L. Prince, "Adaptive fuzzy segmentation of magnetic resonance images," *IEEE Transactions on Medical Imaging*, vol. 18, no. 9, pp. 737–752, 1999.
- [31] M. Nielsen, L. Florack and R. Deriche, "Regularization, scale-space, and edge detection filters," *Journal of Mathematical Imaging and Vision*, vol. 7, no. 4, pp. 291–307, 1997.
- [32] —, "Regularization and scale space," *Technical Report 2352, INRIA, Sophia-Antipolis, France.*, 1994.
- [33] K. Ni, X. Bresson, T. Chan, and S. Esedoglu, "Local histogram based segmentation using the wasserstein distance," *International Journal of Computer Vision*, vol. 84, no. 1, pp. 97–111, 2009.
- [34] K. He, J. Sun, and X. Tang, "Guided image Filtering," *In Computer Vision-[ECCV 2010], K. Daniilidis, P. Maragos, N. Paragios (Eds.), Lecture Notes in Computer Science*, vol. 6311, pp. 1–14, Springer(2010).